Artificial Tripeptide Scaffolds for Self-Assembly of Heteromultimetallic Structures with Tunable Electronic and Magnetic Properties

Brian P. Gilmartin, Rebekah L. McLaughlin, and Mary Elizabeth Williams*

Department of Chemistry, The Pennsylvania State University, 104 Chemistry Building, University Park, Pennsylvania 16802

Received July 1, 2005. Revised Manuscript Received August 21, 2005

An artificial tripeptide containing pendant pyridine and bipyridine ligands has been synthesized using a solution-phase method analogous to divergent dendrimer synthesis, yielding a palindromic multifunctional peptide chain. When compared to conventional solid-phase peptide synthesis, this method rapidly yields the tripeptide in significantly greater quantities. The pendant pyridine ligands are coordinated with stoichiometric quantities of either $[Pt(tpy)]^{2+}$ or [Cu(pda)] metal complexes. By addition of a second transition-metal ion, supramolecular structures are formed by chelation of the bipyridine ligands to create cross-links between oligopeptide strands. The resulting heteromultimetallic materials have unique optical, electrochemical, and magnetic properties that can be tuned by the choice of transition-metal ions.

Introduction

Peptide nucleic acids (PNAs) are structural mimics of deoxyribonucleic acid (DNA) that replace the sugar phosphate with a poly(aminoethylglycine) (aeg) backbone[1] and have a great deal of synthetic versatility based on straightforward synthetic modifications that are not possible in natural DNA.[2] For example, in addition to the incorporation of amino acid residues and nucleobases, nonnatural base pairs[3] and metal-binding ligands[4] have been inserted into the PNA backbone. These variations increase the number of structural motifs for the assembly of double-stranded PNA−PNA or PNA−DNA duplexes and enable the synthetic tunability of their physical properties. Further synthetic modifications should enable a wider variety of biocompatible, peptide-based materials for applications in sensors and pharmaceuticals or as a new motif for self-assembly of nanostructures.

We have recently reported the synthesis of artificial peptides based on the PNA backbone which contained a homosubstituted polyamide chain with a single type of chelating ligand, either monodentate pyridine or bidentate bipyridine.[5] These oligopeptides were shown to bind stoichiometric quantities of transition-metal ions, which resulted in the formation of multimetallic structures. Because the oligopeptides contained the same ligand, the resulting materials contained multiple copies of the same metal complex tethered in close proximity along a peptide scaffold. In those studies,[5] the metal-binding oligopeptides were prepared via solid-phase peptide synthesis, a common approach in which peptides are initiated and sequentially extended while tethered to a solid resin support. Isolation of the desired product from reactants and deletion sequences is relatively facile using this strategy. However, we observed in our earlier report that the artificial oligopeptide yield was typically poor; the optimized synthesis of a tripeptide containing three bipyridine ligands gave only 1.19% yield.[5a] We hypothesized that our yields were negatively affected by the loading of reactive groups on the resin support, the degree of solvation, and aggregation of longer or aromatic-containing sequences.[6] To enable the study of these materials in a variety of electrochemical, spectroscopic, structural, and biophysical experiments, we have sought an alternative route toward the preparation of our ligand-containing artificial oligopeptides that would enable the rapid production of a larger quantity of the desired peptide scaffold.

Inspiration for a more efficient synthesis scheme was derived from the divergent synthetic approach for preparation of dendrimers in which the supramolecular structures are constructed from the core outward.[7] One of the coupling

* To whom correspondence should be addressed. E-mail: mbw@chem.psu.edu.

(1) (a) Nielsen, P. E.; Egholm, M.; Berg, R. H.; Buchardt, O. *Science* **1991**, *254*, 1497−1500. (b) Nielsen, P. E.; Egholm, M.; Buchardt, O. *Bioconjugate Chem.* **1994**, *5*, 3−7. (c) Dueholm, K. L.; Egholm, M.; Behrens, C.; Christensen, L.; Hansen, H. F.; Vulpius, T.; Petersen, K. H.; Berg, R. H.; Nielsen, P. E.; Buchardt, O. *J. Org. Chem.* **1994**, *59*, 5767−5773. (d) Betts, L.; Josey, J. A.; Veal, J. M.; Jordan, S. R. *Science* **1995**, *270*, 1838−1841.

(2) (a) Vernille, J. P.; Kovell, L. C.; Schneider, J. W. *Bioconjugate Chem.* **2004**, *15*, 1314−1321. (b) Ninomiya, K.; Minohata, T.; Nishimura, M.; Sisido, M. *J. Am. Chem. Soc.* **2004**, *126*, 15984−15989. (c) Diaz-Mochon, J. J.; Bialy, L.; Bradley, M. *Org. Lett.* **2004**, *6*, 1127−1129.

(3) (a) Hollenstein, M.; Leumann, C. J. *J. Org. Chem.* **2005**, *70*, 3205−3217. (b) Neuner, P.; Monaci, P. *Bioconjugate Chem.* **2002**, *13*, 676−678. (c) Okamoto, A.; Tanabe, K.; Saito, I. *Org. Lett.* **2001**, *3*, 925−927. (d) Olsen, A. G.; Dahla, O.; Nielsen, P. E. *Bioorg. Med. Chem. Lett.* **2004**, *14*, 1551−1554.

(4) (a) Mokhir, A.; Krämer, R.; Wolf, H. *J. Am. Chem. Soc.* **2004**, *126*, 6208−6209. (b) Mokhir, A.; Stiebing, R.; Kraemer, R *Bioorg. Med. Chem. Lett.* **2003**, *13*, 1399−1401. (c) Popescu, D.-L.; Parolin, T. J.; Achim, C. *J. Am. Chem. Soc.* **2003**, *125*, 6354−6355. (d) Verheijen, J. C.; van der Marel, G. A.; van Boom, J. H.; Metzler-Nolte, N. *Bioconjugate Chem.* **2000**, *11*, 741−743.

(5) (a) Gilmartin, B. P.; Ohr, K.; McLaughlin, R. L.; Koerner, R.; Williams, M. E. *J. Am. Chem. Soc.* **2005,** *127*, 9546−9555. (b) Ohr, K.; Gilmartin, B. P.; Williams, M. E. *Inorg. Chem.*, in press.

(6) (a) Cilli, E. M.; Oliveira, E.; Marchetto, R.; Nakaie, C. R. *J. Org. Chem.* **1996**, *61*, 8992−9000. (b) Krchnák, V.; Flegelová, Z.; Vágner, J. *Int. J. Pept. Protein Res.* **1993**, *42*, 450−454. (c) Fields, G. B.; Fields, C. G. *J. Am. Chem. Soc.* **1991**, *113*, 4202−4207.

(7) Zeng, F.; Zimmerman, S. C. *Chem. Rev.* **1997**, *97*, 1681−1712.

10.1021/cm051435u CCC: $30.25
Published on Web 09/23/2005

chemistries for the growth of successive generations is the formation of amide linkages,[8] and it has recently been shown that a variety of peptide dendrimers may be prepared in this manner.[9] A similar solution-based synthetic approach, focusing on the sequential growth outward from the center of the peptide chain would therefore be a feasible and potentially advantageous way to overcome the limitations of resin-supported synthesis. We subsequently rely on an approach taken by chelation-based dendrimer syntheses[10] to prepare supramolecular structures by linking together the peptide strands with metal coordination chemistry.

In this paper we present a one-pot, solution-based synthesis of an artificial tripeptide with pendant metal-binding ligands in larger yields and on a relatively shorter time scale than typical solid-phase approaches. The central unit for the peptide is diethylenetriamine (DETA), protected at the terminal amines with 9-fluorenylmethoxycarbonyl (Fmoc), and to which a pendant 2,2′-bipyridine (bpy) is linked. Following Fmoc deprotection, coupling chemistry is simultaneously performed on both ends of the chain to link a pyridine (py)-modified aeg monomer (Fmoc-aeg(py)-OH·HCl).[5] This paper is the first report of multifunctional tripeptides that contain ligands with differing denticity and therefore reactivity toward metal complexation. Importantly, this approach also enables the facile preparation of peptides that are palindromic, eliminating one source of geometric isomers.[5] By sequential exposure to different transition-metal ions or complexes, we demonstrate the use of this tripeptide to create a series of heterometallic structures, each of which has unique optical and electrochemical properties that are characteristic of both metal centers tethered to the peptide scaffold.

Experimental Section

Chemicals. All materials were purchased from Aldrich and used as received unless otherwise noted. Ultrapure water (Barnstead, 18.2 MΩ) was used for all experiments; 4′-methyl-2,2′-bipyridine-4-acetic acid (bpyCH_2CO_2H),[11] py-substituted aeg monomer (Fmoc-aeg(py)-OH·HCl),[5] iodo(2,2′:6′,2″-terpyridine)platinum(II) iodine dihydrate (i.e., [Pt(tpy)I]I·$2H_2O$),[12] and aqua(pyridine-2,6-dicarboxylato)copper(II) (i.e., [Cu(pda)(H_2O)])[13] were prepared according to previously published procedures. Tetrabutylammonium hexafluorophosphate (TBAH; Apollo Scientific) was recrystallized three times from ethyl acetate (EtOAc, VWR).

Instrumentation and Analysis. Electrochemical measurements were performed using a CH Instruments potentiostat (model 660A) under an inert atmosphere in a glovebox (MBraun LabMaster 130) using either a 12.5 μm radius Pt or a 1.0 mm radius Pt working electrode, a Ag/Ag^+ reference electrode, and a Pt counter electrode. The working electrode was polished using aqueous slurries of progressively finer grits of alumina (Buehler), rinsed with water and ethanol, and dried before use.

^{1}H nuclear magnetic resonance (NMR) spectra were obtained from either a Bruker AMX-360 MHz or a Bruker DPX-400 MHz spectrometer. Gradient HMQC specta were obtained on a Bruker DRX 400 operating at 400.13 MHz for ^{1}H; data processing was performed on Topspin NMR software. X-band electron paramagnetic resonance (EPR) spectra were acquired with a 9.5 GHz Bruker eleXsys 500 spectrometer with a liquid He cryostat at 20 K using 8.22 mW power, 100 kHz modulation frequency, and 5 G modulation amplitude. UV−vis absorbance spectra were collected using a Varian Cary 50 spectrophotometer and a 1 cm path length quartz cuvette, and the spectra were manually corrected for background absorption using separately collected spectra of reference solutions.

Positive ion electrospray mass spectrometry (ESI+ MS) was performed at the Penn State Mass Spectrometry Facility using a Mariner mass spectrometer (Perseptive Biosystems). Matrix-assisted laser desorption ionization time-of-flight (MALDI-TOF) mass spectra were acquired with a Waters Micromass MALDI micro MX spectrometer.

Molecular structures were calculated using Hyperchem 6.0 using molecular mechanics (MM+) with atomic charge based electrostatic repulsions, and a Polack−Ribiere conjugate gradient to a minimum energy gradient of 0.01 kcal/mol.

Synthesis. *$(Fmoc)_2$DETA·HCl.* A 100 mL solution of DETA (2.00 mL, 0.0185 mol) and *N*,*N*-diisopropylethylamine (DIPEA; 6.42 mL, 0.0368 mol) in dichloromethane (DCM; VWR) was stirred under N_2. To this was added 12.1 g of (9-fluorenylmethoxycarbonyl)succinimide (Fmoc-OSu; Novabiochem, 0.0371 mol) in 80 mL of DCM over 1 h, and the resulting solution was allowed to stir under N_2 for 16 h. The solution was then shaken vigorously with 50 mL of 1 M HCl, yielding a white precipitate which was isolated by vacuum filtration and dried in vacuo for 16 h. Yield: 4.77 g (44.3%). ^{1}H NMR (400 MHz, d_4-MeOH): δ 3.07 (t, $J = 4$ Hz, 4 H); 3.36 (t, $J = 4$ Hz, 4 H); 4.15 (t, $J = 6$ Hz, 2 H); 4.34 (d, $J = 5$ Hz, 4 H); 7.26 (t, $J = 7$ Hz, 4 H); 7.36 (t, $J = 7$ Hz, 4 H); 7.58 (d, $J = 7$ Hz, 4 H); 7.76 (d, $J = 7$ Hz, 4 H). ESI+ MS (*m*/*z*): calcd, $(M + H)^+ = 548.3$; found, $(M + H)^+ = 548.3$.

$(Fmoc)_2$DETA(bpy)·HCl. A 25 mL solution containing 1.73 g of $(Fmoc)_2$DETA·HCl (0.00296 mol) and 1.27 mL of DIPEA (0.00730 mol) in *N*,*N*-dimethylformamide (DMF; VWR) was stirred under N_2. To this was added 1.02 g of bpyCH_2CO_2H (0.00448 mol), 2.26 g of 2-(1*H*-benzotriazol-1-yl)-1,1,3,3-tetramethyluronium hexafluorophosphate (HBTU; Novabiochem, 0.00596 mol), and 75 mL of DMF. The yellow solution was allowed to stir under N_2 for 16 h and then poured into 1.3 L of 1 M HCl, giving a white precipitate. The solid was collected by vacuum filtration and dried under vacuum for 16 h. Yield: 2.17 g (92.2%). ^{1}H NMR (360 MHz, d_6-DMSO): δ 2.46 (s, 3 H); 3.17 (t, $J = 6$ Hz, 2 H); 3.24 (t, $J = 5$ Hz, 2 H); 3.33 (t, $J = 6$ Hz, 2 H); 3.42 (t, $J = 6$ Hz, 2 H); 3.95 (s, 2 H); 4.18−4.22 (m, $J = 7$ Hz, 2 H); 4.26 (d, $J = 6$ Hz, 2 H); 4.32 (d, $J = 6$ Hz, 2 H); 7.28 (t, $J = 8$ Hz, 4 H); 7.38 (t, $J = 8$ Hz, 4 H); 7.56−7.66 (m, $J = 8$ Hz, 5 H); 7.84−7.87 (m, $J = 8$ Hz, 5 H); 8.37 (s, 1 H); 8.39 (s, 1 H); 8.64 (d, $J = 6$ Hz, 1 H); 8.70 (d, $J = 6$ Hz, 1 H). ESI+ MS (*m*/*z*): calcd, $(M + H)^+ = 758.3$; found, $(M + H)^+ = 758.4$.

*Fmoc-aeg(py)-DETA(bpy)-aeg(py)-Fmoc (Compound **1**).* To a 20 mL solution containing 0.5273 g of $(Fmoc)_2$DETA(bpy)·HCl

(8) (a) Haba, Y.; Harada, A.; Takagishi, T.; Kono, K. *J. Am. Chem. Soc.* **2004**, *126*, 12760−12761. (b) Mattei, S.; Seiler, P.; Diederich, F.; Gramlich, V. *Helv. Chim. Acta* **1995**, *78*, 1904−1912. (d) Newkome, G. R.; Lin, X. *Macromolecules* **1991**, *24*, 1443−1444.
(9) Crespo, L.; Sanclimens, G.; Pons, M.; Giralt, E.; Royo, M.; Albericio, F. *Chem. Rev.* **2005**, *105*, 1663−1681.
(10) (a) Armaroli, N. *Chem. Soc. Rev.* **2001**, *30*, 113−124. (b) Sakamoto, M.; Ueno, A.; Mihara, H. *Chem. Commun.* **2000**, 1741−1742. (c) Newkome, G. R.; He, E.; Moorefield, C. N. *Chem. Rev.* **1999**, *99*, 1689−1746. (d) Sakamoto, M.; Ueno, A.; Mihara, H. *Chem.—Eur. J.* **2001**, *7*, 2449−2458. (e) Gorman, C. B.; Smith, J. C. *J. Am. Chem. Soc.* **2000**, *122*, 9342−9343. (f) Vogtle, F.; Plevoets, M.; Nieger, M.; Azzellini, G. C.; Credi, A.; De Cola, L.; De Marchis, V.; Venturi, M.; Balzani, V. *J. Am. Chem. Soc.* **1999**, *121*, 6290−6298.
(11) Della Ciana, L.; Hamachi, I.; Meyer, T. J. *J. Org. Chem.* **1989**, *54*, 1731−1735.
(12) Annibale, G.; Brandolisio, M.; Pitteri, B. *Polyhedron* **1995**, *14*, 451−453.
(13) Ullah, M. R.; Bhattacharya, P. K. *Indian J. Chem., A* **1991**, 976−978.

(0.664 mmol) in DMF was added 1.60 g of tetrabutylammonium fluoride trihydrate (TBAF·$3H_2O$; 5.06 mmol), and the red solution was sonicated under N_2 for 15 min. A 3.43 g amount of 1-hydroxybenzotriazole (HOBt; 25.4 mmol) was added, forming a yellow solution which was stirred under N_2 for 30 s, and 0.804 g of Fmoc-aeg(py)-OH·HCl (1.62 mmol) and 0.312 g of 1-[(3-dimethylamino)propyl]-3-ethylcarbodiimide (EDC; 1.63 mmol) were subsequently added. This solution was stirred under N_2 for 1 h, and 20 mL of Et_2O (VWR) and 40 mL of EtOAc were added. The solution was purified by extraction with 3 × 50 mL of 5% $NaHCO_3$ and 3 × 50 mL of H_2O; the aqueous washings were discarded. Petroleum ether was then added to the organic layer, giving a white solid which was allowed to precipitate for 16 h.[14] The mother liquor was decanted, and the precipitate was dispersed by sonication in petroleum ether, allowed to settle as a fine white precipitate which was collected by vacuum filtration, and dried in vacuo for 3 h. Yield: 197 mg (24.8%). ^{1}H NMR (360 MHz, d_6-DMSO): δ 2.39 (s, 3 H); 3.16 (t, 4 H), 3.32 (m, 18 H); 3.55 (s 4 H); 4.18−4.32 (m, 6 H); 7.12 (t, 1 H); 7.19 (t, 1 H); 7.30 (t, 4 H); 7.39 (t, 4 H); 7.66 (d, 4 H); 7.87 (d, 4 H); 7.98 (d, 4 H); 8.19 (s, 1 H); 8.27 (s, 1 H); 8.36−8.55 (m, 6 H). Additional confirmation of purity was obtained using gradient HMQC NMR (see the Supporting Information for spectra and analysis). ESI+ MS (*m*/*z*): calcd, $(M + H)^+ = 1196.5$; found, $(M + H)^+ = 1196.5$.

*[Pt(tpy)(py)]-aeg(bpy)-aeg-[Pt(tpy)(py)]$(PF_6)_4$ (Compound **2**).* To a solution containing 0.185 g of [Pt(tpy)I]I·$2H_2O$ (0.258 mmol), 49 mL of acetonitrile (ACN, VWR), and 14 mL of H_2O was added 91.0 mg of $AgNO_3$ (Acros, 0.536 mmol). The solution was stirred vigorously for 5 min and centrifuged to isolate precipitated AgI. The mother liquor was decanted, recentrifuged, and decanted to ensure that all AgI had been removed.[15] The solution was then filtered into a flask containing 0.152 g of **1** (0.127 mmol) and the resulting solution stirred at 40 °C for 1 h. The ACN was then removed under reduced pressure and the product precipitated with saturated aqueous ammonium hexafluorophosphate (NH_4PF_6; Acros) to give an orange solid which was collected and recrystallized from acetone/H_2O. The sample was dried under vacuum for 16 h. Yield: 178 mg (53.3%). A 1.13 mM stock solution of **2** was prepared by dissolution of 178 mg of **2** in 60 mL of acetonitrile and subsequently used for the preparation of compounds **4**−**6**.

*[Fe((py)-aeg(bpy)-aeg(py))$_3$]$(PF_6)_2$ (Compound **3**).* To a 10 mL solution containing 0.101 g of tripeptide **1** (0.0840 mmol) in ACN was added a 3.1 mL amount of 8.91 mM $Fe(ClO_4)_2$ (0.0280 mmol). The red solution was stirred under N_2 for 3 h, the solvent removed under reduced pressure, and a saturated aqueous NH_4PF_6 solution added to yield a red precipitate. The solid was collected by centrifugation, washed with H_2O, and dried under vacuum for 16 h. Yield: 91.9 mg (83.4%).

*[Fe([Pt(tpy)(py)]-aeg(bpy)-aeg-[Pt(tpy(py)])$_3$]$(PF_6)_{14}$ (Compound **4**).* A 20 mL portion of the 1.13 mM solution of **2** (22.6 μmol) was added to a methanolic solution of 52.3 mM $Fe(ClO_4)_2$ (144 μL, 7.53 μmol) and the resulting solution stirred for 16 h under N_2. The volume was reduced by rotary evaporation, and a red solid precipitated upon addition of aqueous NH_4PF_6. The solid was collected by centrifugation, rinsed, and dried under vacuum for 16 h. Yield: 57.4 mg (92.6%). ^{1}H NMR (400 MHz, d_6-DMSO): δ 2.33 (m, 5 H); 2.66 (m, 3 H); 2.72 (s, 2 H); 2.88 (s, 3 H); 3.11−3.73 (br m, 130 H); 3.88−4.48 (br m, 18 H); 7.09−7.45 (br m, 30 H); 7.50−7.92 (br m, 48 H); 7.96 (t, 12H); 8.00−8.43 (m, 15 H); 8.47−8.77 (m, 48 H); 8.79−8.89 (m, 3H); 8.99 (dd, 6 H).

*[Cu([Pt(tpy)(py)]-aeg(bpy)-aeg-[Pt(tpy(py)])$_2$]$(PF_6)_{10}$ (Compound **5**).* A 20 mL portion of the 1.13 mM solution of **2** (0.0226 mmol) was added to a methanolic solution of 17.7 mM $Cu(OAc)_2$·H_2O (144 μL, 0.0112 mmol) and the resulting solution stirred for 16 h. The volume was reduced by rotary evaporation, and a light green colored solid was precipitated using a saturated aqueous solution of NH_4PF_6. The solid was collected by centrifugation, rinsed, and dried under vacuum for 16 h. Yield: 52.9 mg (83.5%). ^{1}H NMR (400 MHz, d_6-DMSO): δ 2.33 (m, 3 H); 2.67 (m, 2 H); 2.89 (s, 1 H); 3.32 (br m, 51 H); 3.54 (m, 2 H); 4.01−4.41 (br m, 11 H); 7.12−7.42 (br m, 20 H); 7.55−7.90 (br m, 32 H); 7.98 (t, 8 H); 8.51−8.75 (m, 32 H); 9.00 (dd, 4 H).

*[Zn([Pt(tpy)(py)]-aeg(bpy)-aeg-[Pt(tpy)(py)])$_2$]$(PF_6)_{10}$ (Compound **6**).* A 20 mL portion of the 1.13 mM solution of **2** (0.0226 mmol) was added to a methanolic solution of 51.8 mM $Zn(OAc)_2$·H_2O (Strem, 634 μL, 0.0113 mmol) and the resulting solution stirred for 16 h. The volume was reduced by rotary evaporation, and saturated aqueous NH_4PF_6 was added to precipitate a yellow solid. The solid was collected by centrifugation, rinsed with H_2O, and dried under vacuum for 16 h. Yield: 55.8 mg (88.0%). ^{1}H NMR (400 MHz, d_6-DMSO): δ 2.32 (m, 3 H); 2.67 (m, 2 H); 2.89 (s, 1 H); 3.01−3.48 (br m, 72 H); 4.09−4.33 (br m, 14 H); 7.12−7.41 (br m, 20 H); 7.60−7.95 (br m, 32 H); 7.98 (t, 8H); 8.01−8.36 (m, 10 H); 8.50−8.73 (m, 32 H); 8.89−8.96 (m, 2 H); 9.00 (dd, 4H).

*[Fe([Cu(pda)(py)-aeg(bpy)-aeg-[Cu(pda)(py)])$_3$]$(PF_6)_2$ (Compound **7**).* A 10 mL solution containing 43.7 mg of **3** (0.0111 mmol) in ACN was added to 3.30 mL of a methanolic solution of 20.3 mM [Cu(pda)(H_2O)] (0.0669 mmol) and the resulting solution allowed to stir for 16 h. The volume was reduced by rotary evaporation and Et_2O added, yielding a maroon precipitate. The solid was collected by centrifugation, rinsed with H_2O, and dried under vacuum for 16 h. Yield: 48.6 mg (82.5%). ^{1}H NMR (400 MHz, d_6-DMSO): δ 2.32 (m, 6 H); 2.66 (m, 3 H); 2.73 (s, 3 H); 2.89 (s, 4 H); 3.02−3.59 (br m, 75 H); 4.01−4.48 (br m, 8 H); 6.76−7.47 (br m, 48 H); 7.56−7.74 (br m, 12 H); 7.77−7.98 (m, 12 H).

Spectrophotometric Titrations. *Formation of **2** by Titration of **1** with [Pt(tpy)]$(NO_3)_2$.* The titration was performed using a Varian Cary 500 double-beam spectrophotometer. To a solution containing 0.879 mg of [Pt(tpy)I]I·$2H_2O$ (1.22 μmol) in 10 mL of 7:2 ACN/H_2O was added 0.622 mg of $AgNO_3$ (3.66 μmol). This solution was stirred vigorously for 5 min and centrifuged to isolate precipitated AgI.[15] The mother liquor was decanted, recentrifuged, decanted again, and finally filtered to ensure removal of all solid AgI. A solution of **1** was then prepared in ACN and filtered. The concentration of the oligopeptide (0.353 mM) was determined from its molar extinction coefficient ($\epsilon = 15119\ M^{-1}\ cm^{-1}$) at 379 nm. This solution was titrated into 2.5 mL of the $[Pt(tpy)]^{2+}$ solution in 15 μL increments, and the solution was stirred at 50 °C for 5 min, followed by 5 min of stirring at room temperature after each addition.[5b] To account for changes in absorption due to sample dilution, an equal volume of ACN was added to the reference cell (containing only the $[Pt(tpy)]^{2+}$) for each iterative addition of oligopeptide. Following the experiment, the oligopeptide/$[Pt(tpy)]^{2+}$ solution was back-titrated with $[Pt(tpy)]^{2+}$ to reach the equivalence point, and this solution was stirred at 50 °C for 15 min and at room temperature for 5 min.

*Formation of **4** by Titration of **2** with $Fe(ClO_4)_2$.* A 31.5 μM solution of the $[Pt(tpy)]^{2+}$-functionalized oligopeptide, compound **2**, was prepared by serial dilution from the previous titration. A solution of 0.263 mM $Fe(ClO_4)_2$ was prepared in ACN and titrated into 2.5 mL of the $[Pt(tpy)]^{2+}$/oligopeptide solution in 10 or 100 μL increments. After each addition, the solution was allowed to stir for 15 min, and UV−vis absorbance spectra were obtained.

(14) Ueki, M.; Tsurusaki, T.; Okumura, J. *Pept. Chem.* **1995**, *32*, 213−216.
(15) Lowe, G.; Vilaivan, T. *J. Chem. Res.* **1996**, 386-387.

Scheme 1. Synthesis of the Mixed-Ligand Tripeptide

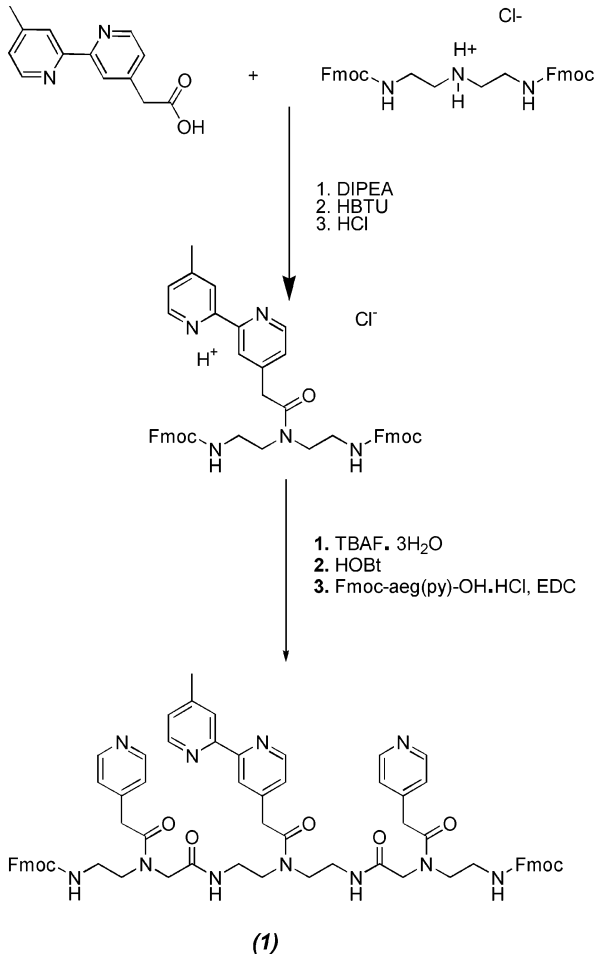

(1)

Results and Discussion

Synthesis of Heterofunctionalized Tripeptides. In our previous reports,[5] the use of solid-phase peptide synthesis enabled the preparation of molecules with multiple ligands tethered to an oligopeptide backbone. To increase the synthetic yield, rapidly produce multifunctional peptides, and eliminate the asymmetry of the different *N*- and *C*-termini on the chain, we have developed an alternative approach to prepare these artificial oligopeptides. We have instead designed palindromic oligopeptides that are easily prepared in solution rather than requiring the use of a solid resin support. DETA, which contains a central secondary amine and two terminal primary amines, was chosen because of its adaptability to our previously developed synthetic methods; Scheme 1 shows the method by which the central monomeric unit is prepared from DETA and a monocarboxylated bpy ligand. To covalently link the bpy ligand to the DETA secondary amine of DETA, it was first necessary to protect the two terminal amines by adding stoichiometric amounts of Fmoc-OSu and DIPEA to a stirring solution of DETA. Following protonation of the di-Fmoc-protected DETA, bpy was coupled to the secondary amine using HBTU.

Subsequent attachment of two pyridine-modified aeg monomers to either end of the DETA monomer (see Scheme 1) is accomplished in a single-pot reaction in nearly quantitative yield. After TBAF deprotects the terminal amines, HOBt is added to quench free F^- in solution. To ensure complete amide coupling, 2.5 molar equiv of both Fmoc-aeg(py)-OH·HCl and EDC were used, a reduction relative to the (typical) 4-fold molar excess for single-site coupling reaction in solid-phase synthesis. The artificial tripeptide was prepared in >100 mg quantities (25% yield) with high purity using significantly less material (solvents, reagents, etc.) and in a relatively shorter time. Importantly, the resulting tripeptide, compound **1**, is both heterofunctional and symmetrically substituted along its backbone. While this approach can be used to prepare oligopeptides containing *any* two similarly substituted ligands, and extended to longer sequences by subsequent coupling reactions,[16] in this study we chose to prepare and fully characterize tripeptides containing bpy and py ligands on the basis of their well-known coordination chemistry with several metallic species and to make connections to our earlier study.[5a]

Spectrophotometric Titration of Tripeptide. Because the pendant ligands have different denticities on the tripeptide backbone, judicious choice of the order with which metal ions or complexes are added can create a library of heterometallic, multinuclear compounds. The two possible routes are shown in Scheme 2. We reasoned that tetracoordinate metal ions bearing a tridentate ligand (i.e., $[Pt(tpy)]^{2+}$ and Cu(pda)) should preferentially bind to the pyridine ligands to fulfill their preferred coordination geometry. Unligated metal ions (Fe^{2+}, Cu^{2+}, and Zn^{2+}) should alternatively bind to the pendant bpy ligands; site-specific coordination is expected both because the bpy ligands are the only vacant sites on the peptide and on the basis of the larger binding affinity of the bidentate (vs monodentate) ligands. To test this method, we first performed spectrophotometric titrations of tripeptide **1** with the complex $[Pt(tpy)]^{2+}$, which we have shown previously binds strongly and in stoichiometric quantities to pyridine-substituted oligopeptides.[5b] The $[Pt(tpy)(py)]^{2+}$ complex has large extinction at distinct wavelengths in the UV region of the spectrum, making observation of complexation of $[Pt(tpy)]^{2+}$ to py straightforward.[17] The difference spectra shown in Figure 1A were acquired during the titration of $[Pt(tpy)]^{2+}$ with tripeptide **1**; the figure shows the increase in the intensity of the characteristic metal-to-ligand charge transfer (MLCT) absorbance at 348 nm following each iterative addition. The MLCT absorption increases and remains constant at a molar ratio of ~2 equiv of $[Pt(tpy)]^{2+}$ per oligopeptide. This ratio is consistent with the stoichiometric addition of two $[Pt(tpy)]^{2+}$ ions to the peptide at each of the pyridine ligands, shown in Scheme 2 as compound **2**.

In this dimetalated peptide, an unmetalated bpy ligand remains available for complexation to another metal ion. Titration of this molecule with additional transition-metal ions would therefore create a heterometallic structure. To be able to again monitor this by UV−vis absorption spectroscopy, we performed a second titration with Fe^{2+},

(16) Morgan, C. M.; Gilmartin, B. P.; Pantzar, L. M. (The Pennsylvania State University). Unpublished results, 2005.
(17) Yutaka, T.; Mori, I.; Kurihara, M.; Mizutani, J.; Tamai, N.; Kawai, T.; Irie, M.; Nishihara, H. *Inorg. Chem.* **2002**, *41*, 7143−7150.

Scheme 2. Synthesis of Heteromultimetallic Tripeptides

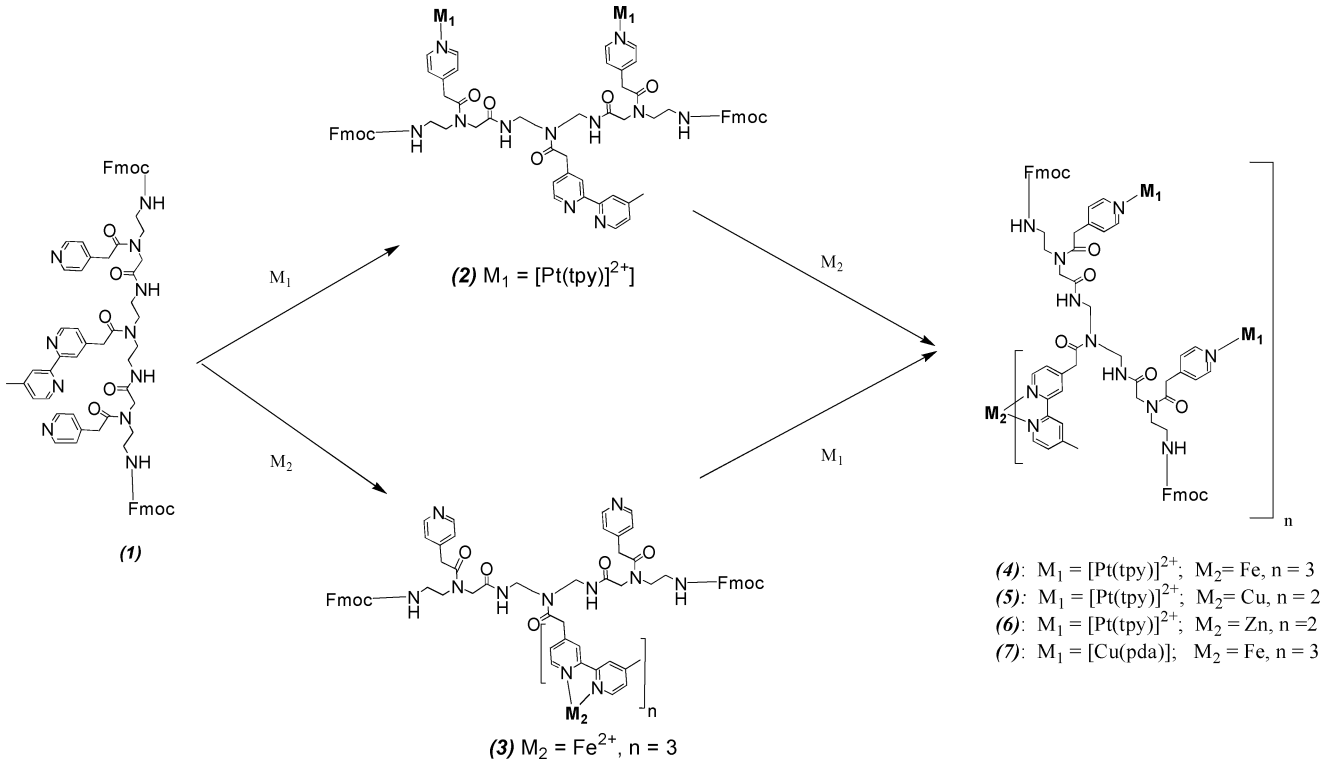

which would be expected to strongly bind any uncoordinated bpy ligands. Figure 1B shows the difference spectra acquired during the titration of **2** with Fe^{2+}; the iterative additions cause the evolution of spectra with increased absorption intensity and a peak at 538 nm, which is attributed to the well-known MLCT band of $[Fe(bpy)_3]^{2+}$.[18] The inset of Figure 1B shows that the peak intensity at 538 nm increases and levels off at a molar ratio of ~0.3 Fe^{2+} to 1 tripeptide. Because Fe^{2+} is known to preferentially form tris(bipyridine) complexes, this result implies that one Fe^{2+} ion cross-links three oligopeptide strands: the resulting heterometallic structure is a peptide-based, supramolecular structure containing six pendant $[Pt(tpy)(py)]^{2+}$ complexes, compound **4** (Scheme 2).

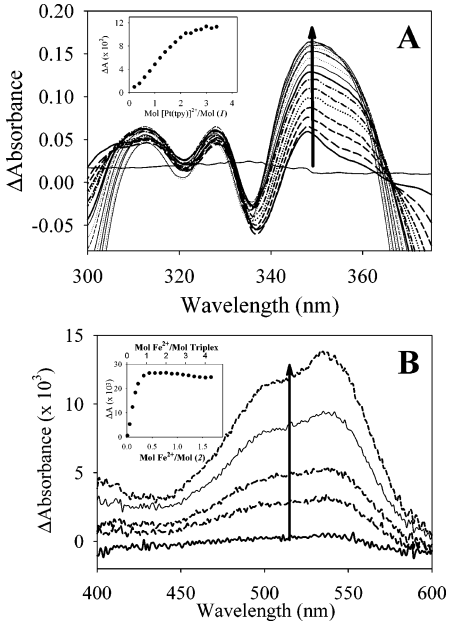

Figure 1. UV−vis absorption difference spectra acquired during (A) the titration of $[Pt(tpy)(H_2O)](NO_3)_2$ with **1** and (B) the subsequent titration of that product (i.e., the $[Pt(tpy)]^{2+}$-coordinated oligopeptide) with $Fe(ClO_4)_2$. Solutions were in ACN and the spectra plotted as the change in absorption vs a reference solution containing a molar equivalent of metal ion in the absence of oligopeptide. Insets: Change in absorption for each iterative addition, at (A) 348 nm and (B) 538 nm, plotted against the molar ratio of metal to peptide or complex.

Formation of Heteromultimetallic Complexes. We utilized a similar strategy of sequential complexation with different metal ions and complexes to prepare a series of complexes. Spectrophotometric titration of **2** with Cu^{2+} and Zn^{2+} is difficult to observe because of their significantly smaller extinction coefficients. Therefore, we prepared the analogous heterometallic complexes of these metals by adding stoichiometric quantities of Zn^{2+} and Cu^{2+} to the diplatinated tripeptide **2**. The resulting complexes, which each contain four $[Pt(tpy)(py)]^{2+}$ complexes tethered to two peptide strands that are cross-linked by either $[Zn(bpy)_2]^{2+}$ or $[Cu(bpy)_2]^{2+}$, were isolated by precipitation from an aqueous solution containing saturated NH_4PF_6, yielding compounds **5** and **6** as their hexafluorophosphate salts.

To test our ability to first coordinate the central bpy ligand (i.e., the alternative route in Scheme 2), the tripeptide was reacted with Fe^{2+} in a molar ratio of peptide to metal of 3:1 (following the experimentally determined stoichiometric quantity above), again producing the dark red color characteristic of $[Fe(bpy)_3]^{2+}$ complexes. This product was isolated and purified by precipitation with NH_4PF_6 before it was reacted with the complex $[Cu(pda)(H_2O)]$, which we have previously demonstrated will stoichiometrically bind to

(18) Lever, A. B. P. *Inorganic Electronic Spectroscopy*; Elsevier Publishing Co.: New York, 1968.

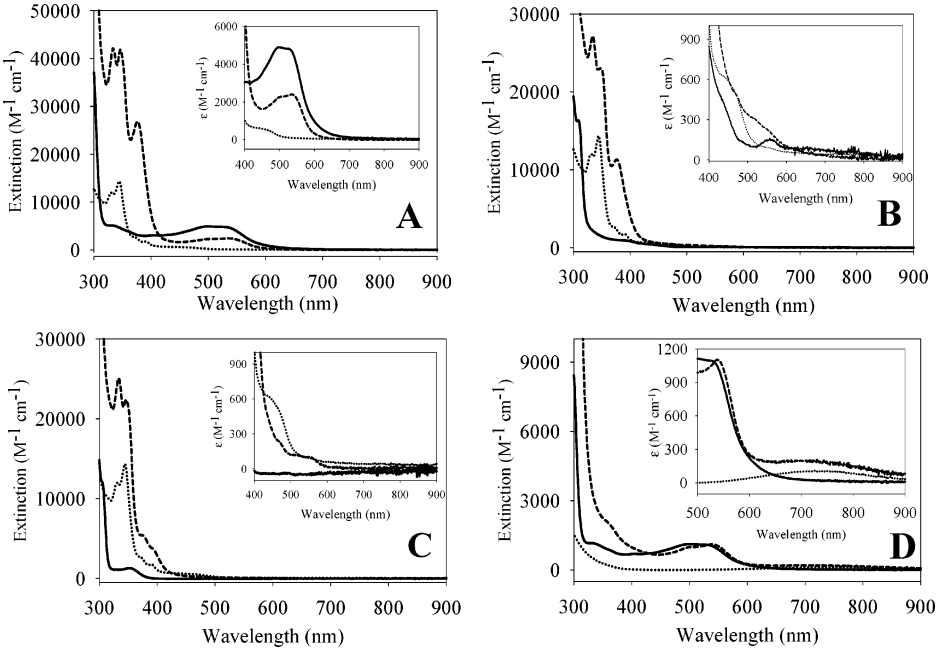

Figure 2. UV−vis absorbance spectra of heterometallic assemblies and respective small-molecule components: (A) compound **4** (---) with $[Fe(Me_2bpy)_3]^{2+}$ (—) and $[Pt(tpy)(py)]^{2+}$ (···); (B) compound **5** (---) with $[Cu(Me_2bpy)_2]^{2+}$ (—) and $[Pt(tpy)(py)]^{2+}$ (···); (C) compound **6** (---) with $[Zn(Me_2bpy)_2]^{2+}$ (—) and $[Pt(tpy)(py)]^{2+}$ (···); (D) compound **7** (---) with $[Fe(Me_2bpy)_3]^{2+}$ (—) and [Cu(pda)(py)] (···). All spectra were normalized for complex concentration in DMF solutions. The insets contain expanded regions of the visible part of the spectrum.

pyridines on the oligopeptide backbone.[5] The resulting complex **7** (in Scheme 2), which contains six [Cu(pda)(py)] complexes tethered to peptide strands that are linked by a central $[Fe(bpy)_3]^{2+}$ complex, was precipitated by the addition of ether.

Validation of this method of preparation of heterometallic oligopeptides is gained by examination of their purity and identity using ^{1}H NMR. The peaks in the ^{1}H NMR spectra of the metalated complexes are broadened because of the increased T_2 relaxation times, a consequence of the large size of the molecules. In addition, the flexible nature of the peptide backbone makes it possible for several solution conformations that give rise to slightly different environments for otherwise equivalent protons. While 2D NMR spectroscopic techniques are useful for determination of the metalated oligopeptide sequence,[19] and in some cases structure, those experiments are complicated by the presence of paramagnetic metal ions in some of the materials in this paper. We are however able to assess the purity of the synthesized materials by comparison of the number of aromatic vs aliphatic protons in the 1-D proton NMR spectra. For example, both complexes **5** and **7** contain paramagnetic Cu^{2+}; complexation to this metal center shifts the ligand protons far downfield so that they are not observed in the aromatic region of the spectrum. As a result, the ^{1}H NMR spectrum of complex **5** does not contain peaks associated with the bpy ligand; for complex **7**, the pyridyl protons are absent. These observations confirm stoichiometric complexation of Cu^{2+} to the bpy and py ligands, respectively. In all cases, comparison of the number of aliphatic and aromatic protons is consistent with the number expected for the fully metalated complexes.[20]

Electronic Absorption Spectroscopy. We designed the multimetallic oligopeptides with the expectation that they would have optical, electronic, and magnetic properties that are characteristic of each of the metal complexes from which they are constructed. Each sequence should therefore have unique signatures that may be "read out" using spectroscopic and electrochemical techniques. Therefore, UV−vis absorption spectroscopy was used to additionally confirm the identity of our complexes and conversely to measure the sequence-specific electronic states available in the multimetallic peptides. The spectra for solutions of each of the metalated oligopeptide complexes were obtained and compared to those for their small-molecule components, shown in Figure 2. The spectra for complexes **4**−***6*** (Figure 2A−C) contain distinctive peaks at 333 and 347 nm that also appear in the spectrum for $[Pt(tpy)(py)]^{2+}$. These peaks are known to result from the MLCT,[17] confirming that **4**−**6** all contain bound $[Pt(tpy)(py)]^{2+}$ moieties. The extinction of the [Pt(tpy)(py)] MLCT absorption in compound **4** is ∼1.5× greater than that in **5** and **6**; this difference is expected because of its larger number of Pt complexes.

The spectra for compounds **4** and **7** (Figure 2A,D) also have visible absorption peaks centered at a wavelength of 537 nm that correspond to the MLCT band observed for $[Fe(bpy)_3]^{2+}$,[18,21] confirming the presence of this species in these structures. While the extinction coefficient for this band in $[Fe(bpy)_3]^{2+}$ complexes is large, the size of the MLCT peak in Figure 2A is overshadowed by the $[Pt(tpy)(py)]^{2+}$ transitions, which are present in a larger quantity than the peptide scaffold. In the case of **7**, the weak absorption peak observed

(19) McLaughlin, R. L. (The Pennsylvania State University). Unpublished results, 2005.

(20) Some of the spectra indicate the presence of H_2O, which is expected to be highly coordinating for Cu^{2+}, Pt^{2+}, and Zn^{2+}, which typically form bis(aquo) complexes. Those protons are taken into consideration for the NMR data analysis.

(21) Hong, Y.-R.; Gorman, C. B. *J. Org. Chem.* **2003**, *68*, 9019−9025.

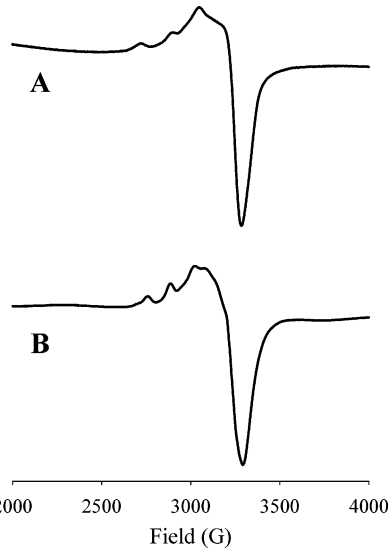

Figure 3. X-band EPR spectra of frozen solutions of (A) 0.85 mM **4** and (B) 0.22 mM **7** in DMF.

Table 1. EPR Parameters and Hyperfine Coupling Constants for Oligopeptide Assemblies 5 and 7

compd	Cu center	Cu/oligopeptide complex	$g_\perp$	$g_\parallel$	$A_\parallel \times 10^{-4}$ (cm^{-1})
5	$[Cu(bpy)_2]^{2+}$	**1**	2.08	2.24	165
7	[Cu(pda)(py)]	**6**	2.09	2.27	131

at 740 nm is due to the ligand-to-metal charge transfer (LMCT) band of [Cu(pda)(py)].[5,13] As expected, there are no observable peaks in the UV−vis region of the spectrum for **6** that correspond to the colorless $[Zn(bpy)_2]^{2+}$ complex. In all cases, the electronic absorption spectra of compounds **4**−**7** are consistent with the linear combinations of the spectra obtained of their small-molecule components using the stoichiometry of the relative ratios of the metal complexes tethered by the peptide backbone.

Electron Paramagnetic Resonance Spectroscopy. Two of the metalated oligopeptides contain paramagnetic metals, which gave characteristic shifts in the ^1H NMR spectra (vide supra): **5** and **7** each contain Cu^{2+} complexes with unpaired electrons whose environments can also be probed using electron paramagnetic resonance (EPR) spectroscopy. Figure 3 contains EPR spectra obtained from frozen DMF solutions of each of these complexes. The larger signal-to-noise ratio in the spectra of complex **7** vs **5** arises from the larger number of bound Cu^{2+} centers per oligopeptide: for **5**, there is a single Cu^{2+}, whereas complex **7** contains six Cu^{2+} complexes bound to each tripeptide triplex. In addition to the magnitudes of the signals, the shapes of the EPR signals are quite different for these two metalated materials. Each of the spectra have the *g* values and hyperfine splitting (Table 1) that are characteristic of Cu^{2+} complexes with square planar geometry ($g_\parallel > 2.1 > g_\perp > 2.0$; $A_\parallel$ is in the range of (158−200) $\times$ 10^{-4} cm^{-1}).[22] However, the smaller hyperfine splitting in **7** is indicative of an oligopeptide containing Cu^{2+} complexes that are (at least weakly) electronically coupled; analysis of this spectrum gives parameters that are similar to those that we have previously reported for a series of pyridine-substituted oligopeptides containing six bound [Cu(pda)(py)] complexes.[5] The similarity between the spectrum for that homometallic hexamer and the EPR spectra shown here for **7** indicates that the central $[Fe(bpy)_3]^{2+}$ complex has little or no effect on the electronic environment of the pendant Cu^{2+} complexes. The diminution of hyperfine splitting in the spectrum leads to the conclusion that, even in frozen solution, the Cu complexes are only weakly coupled, which likely arises from favorable van der Waals forces that result from $\pi-\pi$ stacking of the aromatic rings of the pda ligand.[5b]

Although the signal is less well defined, the EPR spectrum of complex **4** (Figure 3A) has larger hyperfine splitting, indicative of an electronically isolated Cu^{2+} complex. The shape of this spectrum is nearly identical to that reported for $[Cu(bpy)_2]^{2+}$, which is distorted due to the presence of both the *cis*- and *trans*- isomers of coordinated H_2O ligands.[23] The sensitivity of EPR to detect small changes in the bonding environment is in agreement with the earlier ^1H NMR results that showed that complex **4** (as well as the other tripeptides) contain coordinated H_2O ligands. Finally, the similarity between the EPR spectrum in Figure 3A and that of the small-molecule analogue implies that the presence of the four pendant $[Pt(tpy)(py)]^{2+}$ complexes causes no discernible distortion in the EPR spectrum, again indicating a lack of coupling between the metallic complexes.

Electrochemistry. Analogous to the above spectroscopic methods, unique voltammetric signatures are expected for each of the multimetalated peptides on the basis of the number and type of bound metal complexes. Several of the metals used to decorate the tripeptide backbone have experimentally accessible redox states, so electrochemical methods are used to further characterize these materials. Moreover, electronic communication between adjacent complexes should be readily discernible on the basis of the waveshapes and formal potentials in the voltammetry.

We used microelectrode voltammetry to measure the solution-phase redox behavior of each of the molecules because of the greater flux to these electrode surfaces, which reduces the differences in the voltammograms due to heterogeneous electron-transfer rates.[24] All reactions were carried out in air-free environments to reduce the chemical irreversibility of some of the complexes in the presence of dioxygen.[25] Cyclic voltammograms for **4**−**6**, normalized to the concentration of the metalated materials, are shown in Figure 4: all three of the voltammograms contain two large, sigmoidally shaped reductions with half-wave potentials ($E_{1/2}$) of −0.6 and −1.1 V. These waves are attributed to the two sequential tpy-centered reductions ($tpy^{0/1-}$ and $tpy^{1-/2-}$) and are not observed for complex **7** (not shown). In the voltammogram of compound **4**, the current of the first reduction wave ($E_{1/2} = -0.60$ V) is 50% larger than observed

(22) (a) Lucchesse, B.; Humphreys, K. J.; Lee, D.-H.; Incarvito, C. D.; Sommer, R. D.; Rheingold, A. L.; Karlin, K. D. *Inorg. Chem.* **2004**, *43*, 5987−5998. (b) Wei, N.; Murthy, N. N.; Karlin, K. D. *Inorg. Chem.* **1994**, *33*, 6093−6100.

(23) (a) Garribba, E.; Micera, G.; Sanna, D.; Strinna-Erre, L. *Inorg. Chim. Acta* **2000**, *299*, 253−261. (b) Noack, M.; Gordon, G. *J. Chem. Phys.* **1968**, *48*, 2689−2699.

(24) Bard, A. J.; Faulkner, L. R. *Electrochemical Methods, Fundamentals and Applications*, 2nd ed.; John Wiley & Sons: New York, 2001.

(25) Hill, M. G.; Bailey, J. A.; Miskowski, V. M.; Gray, H. B. *Inorg. Chem.* **1996**, *35*, 4585−4590.

Table 2. Summary of Electrochemical Data for 4−6[a]

compd	$E°$ (V vs SCE)[b]						$D \times 10^6$ (cm^2/s)	r_H[c] (nm)
	$Fe^{3+/2+}$	$Cu^{2+/1+}$	$tpy^{0/1-}$	$tpy^{1-/2-}$	$bpy^{0/1-}$	$bpy^{1-/2-}$		
4	+0.96		−0.59	−1.16			3.5	7.9
5		+0.36	−0.62	−1.15			5.8	4.7
6			−0.64	−1.12			5.5	4.9
$[Fe(bpy)_3]^{2+}$	+0.95				−1.10	−1.30	13.5	2.0
$[Pt(tpy)(py)]^{2+}$			−0.65	−1.12			15.7	1.7
$[Cu(bpy)_2]^{2+}$		+0.28					*d*	*d*
[Cu(pda)(py)]		+0.10					*d*	*d*

[a] All experiments performed in DMF solutions containing 0.25 M TBAH. [b] Formal potentials determined either from the half-wave potential ($\sim E_{1/2}$) in microelectrode cyclic voltammograms (Figure 4) or the average peak potential in macroelectrode voltammograms (not shown). [c] Calculated from the diffusion coefficients using eq 2. [d] Not determined because of the electrochemical and chemical irreversibility of these reactions.

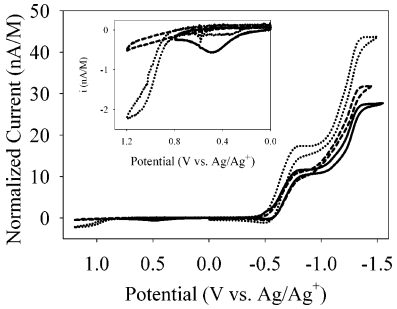

Figure 4. Cyclic voltammograms of **4** (···), **5** (—), and **6** (---), performed with a 25 μm diameter Pt working electrode, a Pt wire counter electrode, and a Ag/Ag^+ reference electrode. All solutions contained 0.25 M TBAH in DMF using a potential scan rate of 50 mV/s. The currents are normalized for the concentration of the complex.

for compounds **5** and **6**, which is a result of **4** containing six pendant $[Pt(tpy)(py)]^{2+}$ moieties vs four in compounds **5** and **6**. In all three compounds, the observed currents for the second tpy reduction ($E_{1/2} = -1.1$ V) are larger than those for the $tpy^{0/1-}$ reaction. Since in the small molecule the tpy reductions are both electrochemically reversible, one-electron reactions, the difference in magnitude in the limiting currents in the voltammograms in Figure 4 is not due to a change in the redox properties of the molecule. Instead, the enhanced currents in the second wave are attributed to an overlapping reduction reaction that is associated with the bpy ligands that are also tethered to the tripeptide. In the small-molecule analogues, the first bpy-centered reduction occurs at an $E_{1/2}$ of −1.1 V and is slightly shifted depending on the metal to which it is coordinated (see Table 2).

Examination of the voltammograms at anodic potentials (Figure 4 inset) indicates clear differences in the oxidation reactions for **4**−**6** that are a result of the variation in the metal forming the $[M(bpy)_n]^{2+}$ peptide cross-link. Complex **4** possesses an oxidative wave at an $E_{1/2}$ of +0.96 V that is attributed to the $Fe^{3+/2+}$ oxidation. Alternatively, the voltammogram of **5** contains an electrochemically irreversible wave, typical for $Cu^{2+/1+}$ reactions because of a conformational change from square planar to tetrahedral during this redox reaction.[26] No oxidation wave is observed in **6**, which is consistent with the known lack of oxidative redox chemistry.

Analysis of the relative magnitudes for each of the redox reactions for a particular heterometallic tripeptide provides a means to assess the relative quantities of the two coordinated metal complexes. For example, careful examination of the cyclic voltammogram for complex **4** indicates that the limiting current (i_{lim}) for the $[Fe(bpy)_3]^{3+/2+}$ reaction is 2.3 μA; for the first tpy reduction of $[Pt(tpy)(py)]^{2+}$ i_{lim} is 15.7 μA.[27] These values are used to quantitatively evaluate the solution transport of these materials using the expression for the limiting current at a microelectrode:[24]

$$i_{lim} = 4nFrDC \quad (1)$$

where n is the number of electrons exchanged in the redox reaction, F is Faraday's constant (96485 C/mol), r is the radius of the microelectrode (cm), D is the molecular diffusion coefficient (cm^2/s), and C is the molecular concentration (mol/cm^3). Since the $[Fe(bpy)_3]^{2+}$ and $[Pt(tpy)(py)]^{2+}$ are linked by the tripeptide scaffold, they possess the same diffusion coefficient. The difference in the amount of observed current for the two reactions (both of which are known to be one-electron processes) is due to the difference in the number of metal complexes per oligopeptide. On the basis of the ratio of the limiting currents, complex **4** contains 1 $[Fe(bpy)_3]$ molecule:6.8 [Pt(tpy)(py)] molecules, consistent with the molar ratio of 1:6 that is confirmed separately. The slight difference may arise from an attenuated Fe oxidative current as a result of its location at the core of this peptide supramolecular structure or slight enhancement of the tpy reduction because of small amounts of O_2 or H_2O in the sample, both of which contribute to the background currents at these potentials. Alternatively, since the multimetallic structure has an overall charge of +14, its mass transport to the positively charged anode may be slowed by electrostatic repulsion. However, the voltammograms contain no evidence for adsorption of these molecules to the electrode surface, so the differences in current are not due to anomolous behavior. Similar analysis of the two metal complexes that comprise each of compounds **5**−**7** is limited because of the electrochemical irreversibility (for the Cu complexes) or lack of a redox wave (for Zn).

The limiting currents observed for the first tpy reduction for compounds **4**−**6** (Figure 4) are used with eq 1 to calculate the diffusion coefficients for these compounds, and these are also given in Table 2. The data show that the calculated diffusion coefficients for compounds **5** and **6** are approximately equivalent, and larger than that of the oligopeptide triplex **4**. To understand these data, we used the energy-minimized structures in Figure 5 to compare the relative

(26) Rorabacher, D. B. *Chem. Rev.* **2004**, *104*, 651−697.

(27) Because of the slight hysteresis in the current for the forward and reverse scans, the limiting current for the reactions is taken as the average of these two.

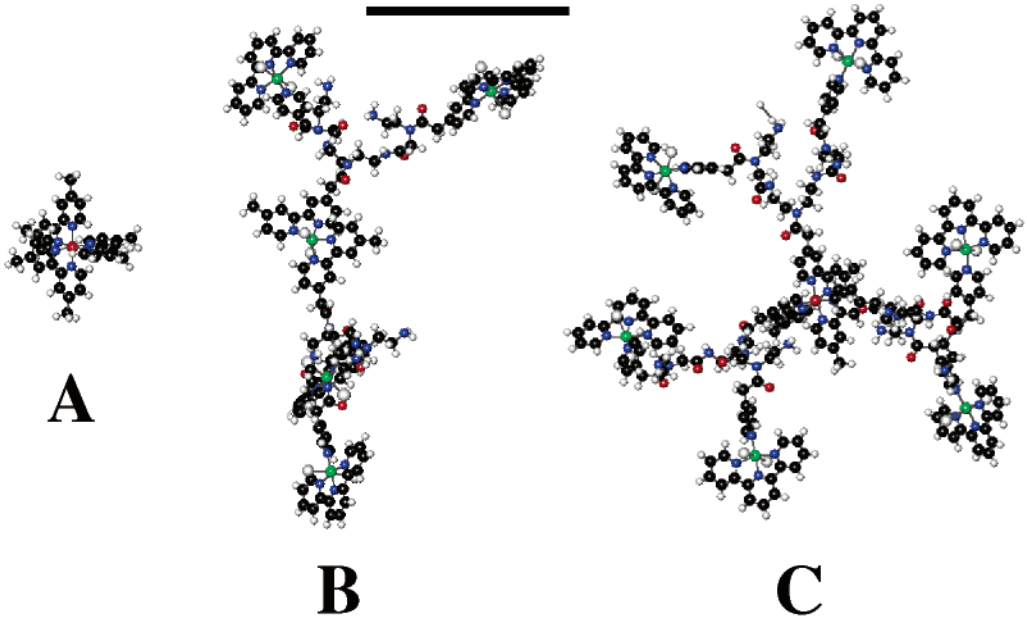

Figure 5. Energy-minimized (MM+) molecular models of (A) $[Fe(Me_2bpy)_3]^{2+}$, (B) compound **5**, and (C) compound **4**, calculated using Hyperchem 6.0. The scale bar indicates 2.0 nm.

molecular sizes. These molecular models show that even though the metal-coordinated peptides are highly flexible in solution, the diameter of the Fe-linked peptide triplex is ~4 times greater than that of the small-molecule analogue $[Fe(Me_2bpy)_3]^{2+}$. Comparison of the electrochemical data shows that the multimetallic structures diffuse 4−5 times slower than their small-molecule analogues (Table 2). The relationship between the molecular size and measured diffusion coefficient is given by the Stokes−Einstein relationship[28]

$$D = k_B T/6\pi r_H \quad (2)$$

where k_b is Boltzmann's constant, T is the absolute temperature, η is the solution viscosity, and r_H is the hydrodynamic radius of the molecule. Thus, the measured D values are used to calculate the hydrodynamic radii for each of the multimetallic peptides, which are also given in Table 2 with the radii calculated for the small-molecule analogues. The calculated r_H values are systematically larger than those predicted by molecular modeling (Figure 5), which is commonly observed in electrochemical measurements because diffusion of the molecule is accompanied by solvent and counterion molecules. However, the relationship between r_H and D for the Cu- or Zn-linked peptide duplexes, compared to the Fe-linked peptide triplex and the small molecules, is consistent with the smaller molecular dimensions in Figure 5B, in support of the understanding of their connectivity to the peptide scaffold.

Acknowledgment. We thank Professor Mike Green and Rachel Behan for assistance with acquisition of the EPR spectra and the Lecomte group for the use of Topsin. We are grateful for the generous financial support of the David and Lucile Packard Foundation Fellowship for Science and Engineering.

Supporting Information Available: Example NMR spectra, including ^{1}H NMR and 2D HMQC NMR, with structural analysis and cyclic voltammograms (PDF). This material is available free of charge via the Internet at http://pubs.acs.org.

CM051435U

(28) Atkins, P.; de Paula, J. *Physical Chemistry*, 7th ed.; W. H. Freeman and Co.: New York, 2002.